Feature-shape and Line-edge Roughness Measurement of Deep sub-micron Lithographic Structures using Small-angle Neutron Scattering

Eric K. Lin[a], Wen-li Wu[a], Qinghuang Lin[b], and Marie Angelopoulos[b]

[a] Polymers Division, National Institute of Standards and Technology, Gaithersburg, MD 20899
[b] IBM T. J. Watson Research Center, Yorktown Heights, NY 10598

ABSTRACT

We demonstrate the application of small angle neutron scattering (SANS) measurements for the quick, nondestructive, and quantitative measurement of the feature shape and size and line-edge roughness of lithographically prepared structures using a model photoresist pattern consisting of a periodic grating of 0.15 μm lines. The measurements are performed directly on structures as fabricated on a silicon wafer with no other sample preparation. For well-defined patterns placed normal to the neutron beam, we easily observe up to six orders of diffraction peaks. Analytic expressions from standard small angle scattering formalism are used to extract the average line structure, spacing, and line-edge roughness from the peak positions and intensities. Additional structural information is obtained by tilting the pattern relative to the incident beam. Changes in the observed scattering data as a function of the tilting angle are related to characteristics such as the height of the structures and the symmetry of the line shape.

INTRODUCTION

As next generation microlithography materials and processes are developed to fabricate the smaller features needed for continued improvements in integrated circuit performance; there is a need for metrology tools able to quantitatively characterize the structure and resolution of sub-100 nm features. At these length scales, the resolution requirements for a fabrication process are more stringent. For example, for the sub-100 nm technology node, the critical dimension cannot vary by more than 6 nm. Quantitative measurements of fabricated structures are needed to evaluate and optimize next generation processes and materials.

The predominant tools used by the semiconductor industry have been microscopy-based techniques such as scanning electron microscopy (SEM) [1,2] and atomic force microscopy (AFM) [2-5] or optical scattering methods such as scatterometry [6-8]. These methods are applied to measure quantities such as the critical dimension (CD) of the structures and the line-edge roughness (LER) or the average fluctuations about an average line position. These tools have provided much needed information both on-line and off-line for quality control tests and the evaluation of a given fabrication process. However, for CD's that approach 100 nm and below, significant challenges arise for each of these methods. Quantitative values from SEM measurements require image analysis software and calibration standards to accurately determine LER and CD values from top down images [1, 2]. AFM and other scanning probe techniques often require specialized tools and analysis software to account for effects from the size and shape of the probe tip, particularly for the characterization of sharply delineated structures. Technical advances using AFM include the use of a boot-shaped probe tip [3], cleaving the sample to access the sidewalls of structures [4], and analysis methodologies to deconvolute the effect of the probe tip with the feature edges [5]. Optical scatterometry, the measurement of laser light scattered from a structure as a function of the observation angle, is a diffraction-based methodology developed to provide a quick nondestructive characterization of lithographic structures [6-8]. The observed diffraction pattern may be analyzed using the rigorous coupled wave theory, a vector differential technique for Maxwell's equations [9]. The experimental instrumentation is not overly expensive, but the solution of the equations requires significant computation time. Additionally, available laser wavelengths are not short enough to access scattered intensities other than the zero order diffraction from grating structures that are less than 0.15 μm in size.

As an alternative and complementary method to characterize the feature shape and line-edge roughness of lithographically prepared structures, we have introduced the use of small angle neutron scattering (SANS) measurements

[10]. The SANS method is a diffraction-based methodology that uses a neutron source rather than a photon source, but differs in other significant respects from optical scattering methods. The important advantages of the use of SANS to characterize structures fabricated with microlithography include the following.

- A separate calibration standard is not needed for the measurement because the measured dimensions are dependent upon the wavelength (and wavelength spread) of the neutron beam, an extremely well known quantity. Critical dimensions and feature resolution parameters can be obtained with nanometer resolution.
- As feature sizes decrease to 130 nm and smaller, the instrumental and resolution requirements for SANS become less demanding.
- The fundamental theoretical framework, data reduction, instrumentation, and analysis are well established for a variety of areas in condensed matter physics to study structures with length scales ranging from 1 nm to 100 nm [11].
- The analytic expressions used to analyze the data are relatively simple expressions that depend only on density (contrast to neutrons) variations in the measured structure. Unlike optical scattering, the vector quantities needed to describe the interaction of light with the materials are not needed.
- SANS measurements can be performed in transmission on structures as prepared on silicon substrates with no additional sample preparation because single crystal silicon is transparent to neutrons at these angular ranges.
- It is possible to characterize structures that are inaccessible through microscopy such as structures that contain holes buried within the layer (i.e. nanoporous low-k dielectric materials) or structures that have deep undercuts in them.
- The neutron beam size samples large areas so that averaged information over many different features is obtained. This characterization provides a measure of the overall resolution of a given lithographic material system or processing conditions.

The primary and obvious limitation of the SANS measurement method as a routine characterization method is the requirement of a reactor neutron source. The routine application of SANS in a production line is impractical because of the cost and the infrastructure needed to maintain such a facility. Additionally, the spot size of the neutron beam is too large to determine differences in critical dimensions of structures that are in close proximity to one another. SANS measurements cannot replace traditional on-line characterization methods such as SEM, optical scatterometry, or AFM, because of availability and cost. SANS measurements, however, can serve as a powerful tool to validate calibration standards and is one of few methods able to provide high-resolution metrology for the evaluation of new materials and processes for structural features expected to be smaller than 100 nm in size.

EXPERIMENT

A grating pattern of periodically spaced parallel lines was prepared on a 200 mm silicon wafer using standard chemically amplified photoresist processing. The nominal size of the line structures was 0.15 μm and the thickness of the resist layer was 0.62 μm. The thickness of the resist layer was measured using x-ray reflectometry. Each grating pattern was prepared over an area of 8 mm by 8 mm using the same photomask. A series of patterns were created by developing exposed images after moving the optimal focus in steps of 0.2 μm. The different focus conditions resulted in variations in the final line structures to be measured in the SANS instrument.

The measurements were performed on the 30 m SANS NG7 instrument at the National Institute of Standards and Technology Center for Neutron Research. The neutron wavelength, λ, was 8.44 Å with a wavelength spread of $\Delta\lambda/\lambda = 0.11$. The sample to detector distance was 15.3 m and the final aperture size was 1.27 cm in diameter. The scattered intensity is collected on a two-dimensional detector. For this series of experiments, newly developed neutron focusing optics consisting of 28 biconcave MgF_2 lenses were used to access the scattering angles needed to resolve diffraction from 300 nm periodic patterns [12]. These angles had previously not been accessible for neutron scattering instruments. In this configuration, the accessible range of q, ($q = (4\pi/\lambda)\sin\theta$, where 2θ is the scattering angle) is 0.0011 $Å^{-1}$ to 0.015 $Å^{-1}$. The scattering data are reduced using standard methods. The scattering intensity from the unexposed areas of the photoresist was subtracted from the scattering intensity from the grating patterns. The scattering data were not placed on an absolute intensity scale although there is no experimental difficulty in doing so in the future.

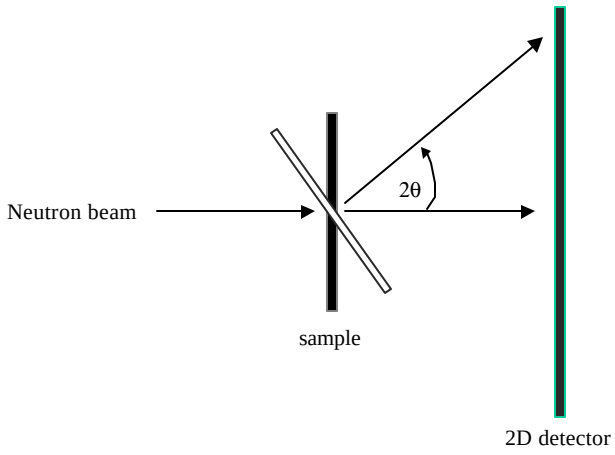

Figure 1. Schematic diagram of a top down view of the experimental setup. The sample is placed directly into the beam either normal to the incident beam (filled) or at an angle to the incident beam (unfilled). The axis of rotation is normal to the page and the line structures are aligned parallel to the axis of rotation.

The sample was placed directly into the neutron beam under ambient conditions without any further sample preparation. A schematic diagram of a top-down view of the experimental configuration is shown in Figure 1. The sample is mounted on a rotation stage so that the angle of the neutron beam on the sample can be well controlled. The axis of rotation for the sample is perpendicular to the page and the line structures are aligned parallel to this axis of rotation. The single crystal silicon wafer is essentially transparent to neutrons and almost all of the observed scattering intensity arises from the grating pattern. We observe significant scattering from a single imaged layer 0.62 μm thick. Up to six hours of counting time were used to obtain good statistics, but 10 minutes of counting time were sufficient to obtain useful data. In contrast, other SANS studies from polymer blend thin films [13] and nanoporous low-k dielectric constant thin films [14] required stacks of six to twenty samples to obtain enough scattering intensity over a reasonable time scale. Significantly, there is sufficient contrast between the photoresist material and the ambient atmosphere to provide a strong scattering signal.

RESULTS AND DISCUSSION

In the first series of experiments, the line patterns are placed normal to the incident neutron beam. In Figure 2, a series of both side view and top view SEM micrographs from the series of focusing conditions are shown along with the raw scattering data from the two dimensional detector. The SEM micrographs clearly show that the focusing conditions result in changes in the shape of the line structures. In the best focus condition, 0.0 μm, and the +0.2 μm condition, the grating structures are well defined with sharp edges. The other two focusing conditions, +0.4 μm and –0.2 μm, result in structures that are more trapezoidal in shape, less defined, and with more line-edge roughness than the 0.0 μm and +0.2 μm structures. The SANS patterns for each of these conditions show six orders of diffraction peaks. The diffuse halo in the center of the SANS images are due to the photoresist material. The diffuse halo is subtracted out from the data before the intensities of the diffraction peaks are analyzed quantitatively. The widths of the observed diffraction peaks are very narrow and can be accounted for by the angular divergence and wavelength spread of the instrument. The peaks are in the horizontal plane of the detector because the lines are vertically oriented with respect to the detector image. The high quality diffraction patterns show that the periodic structure is strongly correlated over the entire beam spot area of several square centimeters. The neutron focusing optics are used to minimize the beam spot on the detector allowing for the resolution of the first order diffraction peak from the 300 nm repeat distance. For a smaller periodic spacing, the diffraction peaks would move farther away from the center of the detector toward larger angles where the SANS resolution requirements are not as stringent. For a larger periodic spacing, the first order diffraction peak may be lost behind the beam stop, but the higher order diffraction peaks would still provide scattering intensities that could be analyzed using the formalism illustrated below.

The diffraction peaks positions are sufficient to obtain some important information about the grating structure such as the overall repeat distance. For the sample prepared under the best focus conditions, the peak position as a function of the diffraction order is shown in Figure 3. The repeat distance can be determined from a linear fit to the data. For this sample, the slope of the line is $(2.07 \times 10^{-3} \pm 6.0 \times 10^{-6})$ Å^{-1} and corresponds with an overall repeat distance of (3031 ± 9) Å [15]. The error bars result from a standard deviation in the linear fit. This distance is slightly greater than but very close to the expected spacing of 3000 Å.

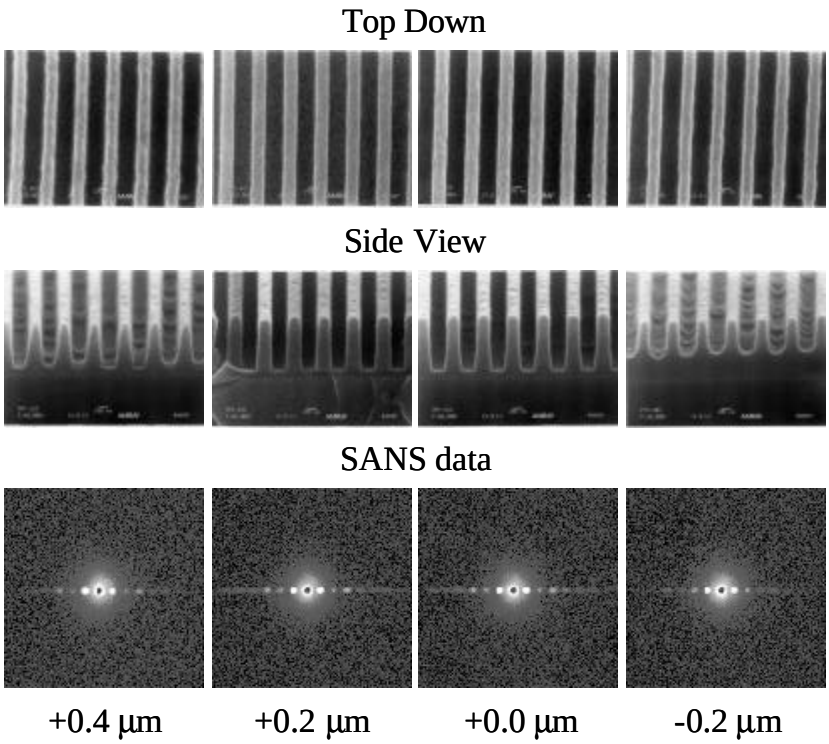

Figure 2. SEM micrographs (top down and side views) and raw SANS data for a series of grating structures prepared lithographically using the same photomask and wafer with varying focal plane distances ± from the optimal focusing conditions (+0.0 μm). The sharply defined peaks indicate that long-range order is present in each area. The diffuse halo near the center of the SANS patterns arises from the photoresist material and is subtracted out before quantitative analysis of the scattered intensities.

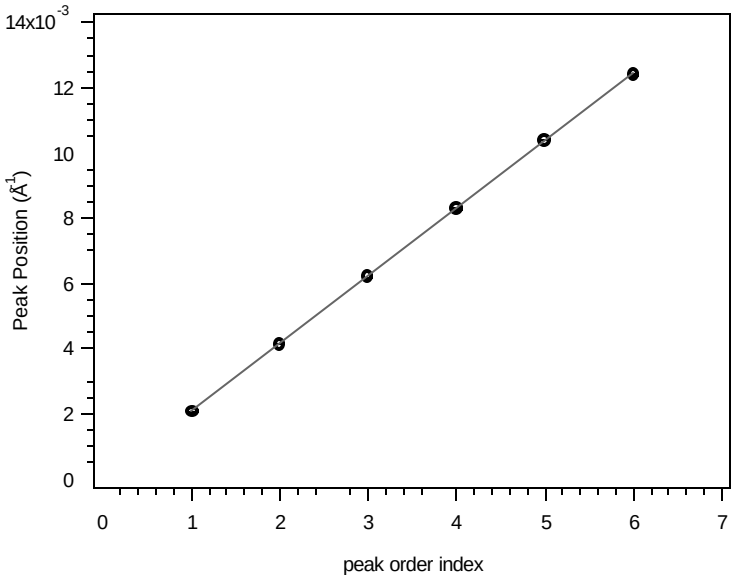

Figure 3. The peak position is shown as a function of the diffraction order. The standard uncertainties in the peak position are smaller than the size of the symbols. The solid line is the best linear fit to the data and provides a quantitative measurement of the repeat distance in the grating pattern.

The scattering data represent the Fourier transform of the real space projection of the grating line structure. In scattering measurements, the phase information of the observed scattered intensity is lost. As a result, a real space description of the structure is constructed and parameters characterizing the model profile are varied to best fit the data. Although a profile is chosen to model the structure, the scattering data is very sensitive to both the symmetry and the characteristic dimensions of the structure.

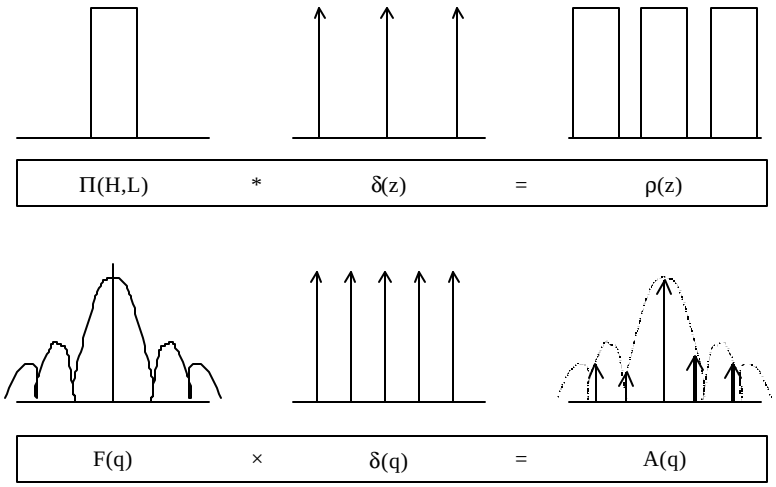

Figure 4. Illustration of the dependence of the scattered intensity on the average cross-section of an average line. In the top row, the cross-section of a given line structure is convoluted with a periodic grating function to model the sample geometry. The bottom row represents the Fourier transforms of each of the real space functions that are observed in a scattering experiment.

The grating structures used in this study are mathematically described in terms of the scattering length density, $\rho(z)$, as a convolution of a periodic grating function, $\delta(z)$, with the cross-sectional profile of a single line structure, $\Pi(H,L)$, or $\rho(z) = \delta(z)^* \Pi(H,L)$. In this example, $\Pi(H,L)$ is a square wave function with a height, H, and a half line width, L. The real space model is written in one dimension because the lines in this study are effectively infinitely parallel in the vertical direction of the detector. The real space model of the line structure is not necessarily the cross-section as seen in the side view SEM micrographs, but represents the projection of the structure onto the plane parallel to the detector. This distinction plays an important role in experiments where the grating structure is tilted relative to the incident neutron beam.

The scattered function, *A(q)*, is simply related to the Fourier transform of the convolution describing the real space profile. Mathematically, the grating function transforms into a grating function in Fourier space, $\delta(q)$, and the shape function, Π, is transformed into a form factor, *F(q)*. The functions are related through the expression, $A(q) = \delta(q)F(q)$. The observed scattering intensities are given by $I(q) = \delta(q)F^2(q)$. The defined grating function results in scattered intensity values that are modulated by the form factor function, *F(q)*. The relationship between the real space profile and the scattering function are schematically illustrated in Figure 4.

The resolution of the final structure or a measure of the line-edge roughness is incorporated by introducing an additional convolution to the form of an individual line with a Gaussian function with a half width of ξ. The full width at half height of the line profile can then be approximated by the expression $2(L^2 + \xi^2)^{1/2}$. The magnitude of the parameter, ξ, provides a measure of line-edge roughness. The value of ξ does not necessarily correspond with LER values determined from SEM or AFM measurements. More explicit comparisons will be made in the future. For the square wave function in this work, the square of the form factor $F^2(q)$ with the Gaussian roughness has a simple analytic expression

$$F^2(q) = 4H^2\left(\frac{\sin Lq}{q}\right)^2 \exp\left(-\frac{q^2\boldsymbol{x}^2}{2}\right). \qquad (1)$$

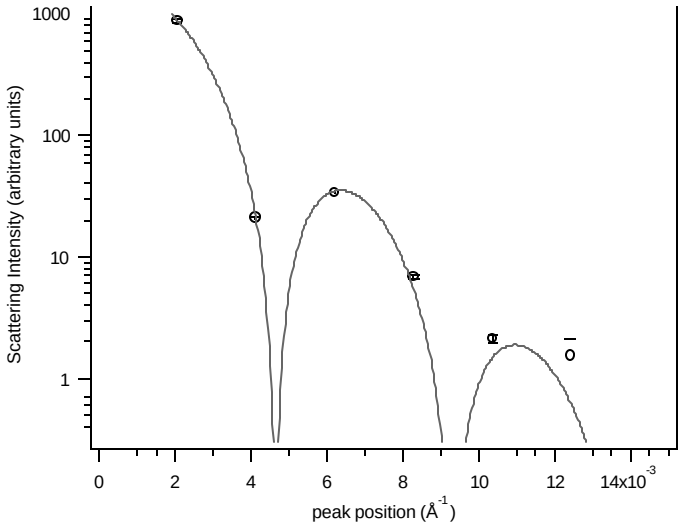

Figure 5. The scattered intensity of each diffraction peak from the best focus condition sample is shown as a function of the peak position in q. The solid line represents the best fit to the peak intensities to the form factor, $F^2(q)$, of a symmetric rectangular structure.

In Figure 5, the form factor expression in Equation 1 is used to fit the scattering intensities at each peak position from the best focus condition sample. The expression in Equation 1 fits the intensity data very well and results in parameter values of L = (675 ± 30) Å and ξ = (213 ± 11) Å. In contrast, fits to the data from the +0.4 μm focusing condition result in parameter values of L = (746 ± 41) Å and ξ = (343 ± 18) Å. These examples show that the line width of an average structure with the best focus condition is slightly narrower than those from the +0.4 μm focusing condition. The effective line-edge roughness of the +0.4 μm focus condition sample is also significantly larger than that from the best focus condition sample. The trends in these structural parameters are qualitatively consistent with the SEM micrographs. In these fits, the parameter values for H were determined as well, but are not presented. The H values do not have a physical meaning because the intensity data were not placed on an absolute intensity scale. In principle, the H parameter would provide the average height of a given structure if the absolute intensity were determined and the chemical composition of the photoresist material were known. Nevertheless, a relative comparison between the H values of these two samples provides a measure of the relative heights of the two line structures because the scattering data were obtained under identical conditions. From these fits, we determine that the average height of the +0.4 μm focusing condition sample is approximately 70 % of the height of the best focusing condition lines.

Thus far, the measured structural information was obtained with the sample grating placed perpendicular to the incident neutron beam. In this section, we illustrate qualitative features in the SANS data that provide additional structural information about the grating structures when the grating pattern is placed at varying angles to the neutron beam. Differences in the SANS data arise because of changes in the projection of the line structure onto the plane parallel to the detector. More three-dimensional information can be obtained about the average line structure such as the symmetry of the profile and the height of the structures. The theoretical framework for the quantitative characterization of the scattered intensities corresponding tilt angles will be developed in the future. In this work, we present the raw scattering data as a function of the sample tilt angle (angle away from the perpendicular configuration) for the best focus condition sample and the +0.4 μm focusing condition sample and discuss qualitative features of these scattering data.

Figure 6 shows a series of data taken from the best focusing condition sample as a function of tilt angle from the sample normal to the neutron beam. As the tilt angle increases from 5° to 25°, the observed diffraction peaks gradually disappear starting with the higher order peaks. The first order peak near the center of the detector remains visible even up to a 25° tilt angle. Although the counting statistics are not as good, the data from the negative tilt angles, -5° and -10°, match the data from +5° and +10° tilt angles. The effect of the rotation on the projection of the grating onto the detector on the scattering data is symmetric around a 0° tilt angle. The continuous decrease in the intensities of the higher order diffraction peaks shows that the projection of the line profile on the plane parallel to the detector is centrosymmetric upon rotation. For this sample, a rectangular profile meets this criterion. An example of a non-centrosymmetric projection upon rotation is shown in Figure 7. Additionally, the angle at which all the diffraction peaks disappear provides an estimate of the height of the line structure relative to the gap spacing.

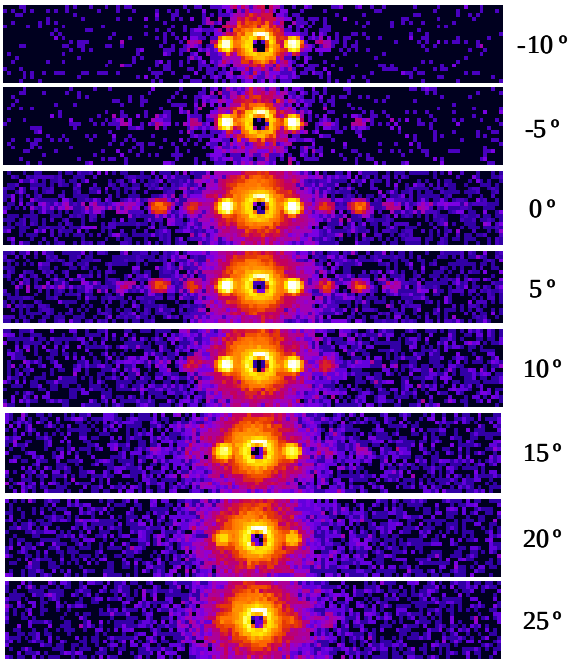

Figure 6. SANS data of the best focusing condition sample taken from a central horizontal slice of the detector as a function of sample tilt angle. The top two angles are counts have fewer counts because the data were collected for 10 minutes instead of 6 hours in the other data.

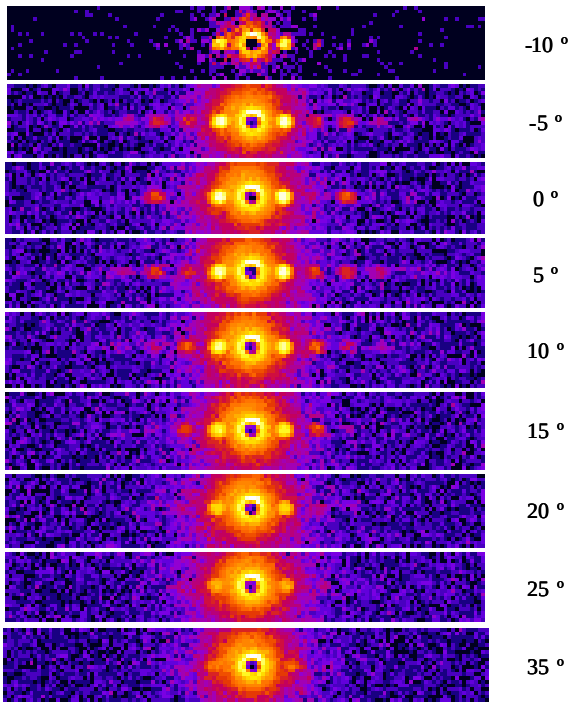

Figure 7. SANS data from the +0.4 μm focusing condition sample taken from the central horizontal slice of the detector as a function of the sample tilt angle. The –10° data set has fewer counts because the data were collected for 10 minutes instead of 6 hours for the other data.

Figure 7 shows a series of data taken from the +0.4 μm focusing condition sample as a function of tilt angle from the sample being normal to the neutron beam. Like the data in Figure 6, as the tilt angle increases from 5° to 25°, the observed diffraction peaks gradually disappear starting with the higher order peaks. Also, the scattering patterns do not depend upon the sign of the tilting angle and are symmetric about 0° tilt. However, unlike the data in Figure 6, the ± 5° tilt diffraction patterns are markedly different from the 0° tilt data. The second and fourth order diffraction peaks are not present in the 0° tilt data, but appear strongly in the ± 5° tilt data. The disappearance of the even order diffraction peaks occurs because minima in the form factor extinguish the diffracted intensity. This occurs when the average critical dimension of the line profile is very near half the overall repeat distance. This is consistent with the fitted average profile from the 0° tilt data where the line width was determined to be (1492 ± 80) Å and the repeat distance was (3031 ± 9) Å. Upon tilting, the even order diffraction peaks reappear because the line profile is better described as a trapezoid rather than a rectangle. The projection of a trapezoidal shape onto the plane parallel to the detector is not centrosymmetric upon rotation. As a result, the form factor of the projected profile onto the detector no long has minima at the diffraction peak positions. Finally, the first order diffraction peak for this sample is present up to a 35° tilt and is consistent with the previous observation that the height of these structure is less than that of the lines in the best focusing condition.

Thus far, quantitative parameters have not been determined from fits to the scattered intensities with rotation. The grating patterns used here simply provide useful examples to illustrate the relatively simple analytic framework needed to extract quantitative information from the SANS data. In principle, any arbitrary shape could be used or studied since the Fourier transform can be performed for any given geometry in a straightforward manner. The structural parameters and line-edge roughness may be obtained by deviations in the scattering data from the targeted structure. In the future, we plan to investigate methods to separately characterize line-edge roughness and sidewall roughness from the SANS data. Varying tilt angles and more in depth analysis of the scattered intensities at all angles should provide much more structural information about the lithographic process. The scattered intensities characterizing sidewall roughness (length scales less than LER) are expected to be lower than the diffraction intensities and are due to inhomogeneities arising from inherent resolution limitations of the fabrication process.

SUMMARY

We have demonstrated the application of SANS for the characterization of lithographically prepared structures as fabricated on a single crystal silicon wafer. SANS provides several advantages over traditional CD and LER metrology methods such as SEM, AFM, and scatterometry. The primary advantage is that requirements on the SANS instrumentation and resolution are relaxed as feature sizes continue to decrease in size. From model periodic grating patterns with a CD of 150 nm and a repeat distance of 300 nm, we show that the feature shape, critical dimension, and LER can be determined from a single photoresist layer with nm resolution over reasonable time scales without any additional sample preparation. Cost and availability limitations preclude routine on-line application of SANS as a metrology tool, but SANS may serve as a powerful technique for the calibration of sub-100 nm standards and for the evaluation of materials or process conditions on the ultimate resolution of a give photolithography process.

ACKNOWLEDGEMENTS

We are grateful to Charles J. Glinka, Paul Butler, Sung-min Choi, and Derek L. Ho of the NCNR at NIST for their help and useful discussion with these measurements. We also acknowledge funding from DARPA under contract N66001-00-C-8803 for support of this work.

REFERENCES

1. H. Marchman, in *Characterization and Metrology for ULSI Technology*, edited by D. G. Seiler, A. C. Diebold, W. M. Bullis, T. J. Shaffner, R. McDonald, and E. J. Walters (American Institute of Physics, College Park, MD, 1998), p. 491.
2. G. W. Reynolds and J. W. Taylor, *J. Vac. Sci. Technol. B*, **17**, 2723 (1999).
3. Y. Martin and K. Wickramasinghe, *Appl. Phys. Lett.*, **64**, 2498 (1994).
4. C. Nelson, S. Plamateer, and T. Lyszczarz, *Proc. SPIE*, **3332**, 19 (1998).
5. G. W. Reynolds and J. W. Taylor, *J. Vac. Sci. Technol. B*, **17**, 334 (1999).
6. C. J. Raymond, M. R. Murnane, S. Sohail H. Naqvi, and J. R. McNeil, *J. Vac. Sci. Technol. B*, **13**, 1484 (1995).
7. S. A. Coulombe and J. R. McNeil, *J. Opt. Soc. Am. A*, **16**, 2904 (1999).
8. I. Kallioniemi, J. Saarinen, and E. Oja, *Appl. Opt.*, **38**, 5920 (1999).
9. T. K. Gaylord and M. G. Moharram, *Proc. IEEE*, **73**, 894 (1985).

10. W. L. Wu, E. K. Lin, Q. H. Lin, and M. Angelopoulos, *J. Appl. Phys.*, **88**, 7298 (2000).
11. R. J. Roe, *Methods of X-ray and Neutron Scattering in Polymer Science*, Oxford University Press, New York, 2000.
12. S. M. Choi, J. G. Barker, C. G. Glinka, Y. T. Cheng, and P. L. Gammel, *J. Appl. Crystallogr.*, **33**, 793 (2000).
13. R. L. Jones, S. K. Kumar, D. L. Ho, R. M. Briber, and T. P. Russell, *Nature*, **400**. 146 (1999).
14. W. L. Wu, W. E. Wallace, E. K. Lin, G. W. Lynn, C. G. Glinka, E. T. Ryan, and H. M. Ho, *J. Appl. Phys.*, **87**, 1193 (2000).
15. All data in the manuscript and in the figures are presented along with the standard uncertainty (±) of the measurement.